

A study on the nature of the peculiar supergiant HD 101584 ^{*} ^{**}

Eric J. Bakker^{1,2}, Henny J.G.L.M. Lamers^{2,1}, L.B.F.M. Waters^{3,4}, Christoffel Waelkens⁵, Norman R. Trams⁶, and Hans van Winckel⁵

¹ Astronomical Institute, University of Utrecht, P.O.Box 80.000, NL-3508 TA Utrecht, The Netherlands

² SRON Laboratory for Space Research Utrecht, Sorbonnelaan 2, NL-3584 CA Utrecht, The Netherlands

³ Astronomical Institute, University of Amsterdam, Kruislaan 403, NL-1098 SJ Amsterdam, The Netherlands

⁴ SRON Laboratory for Space Research Groningen, P.O.Box 800, NL-9700 AV Groningen, The Netherlands

⁵ Astronomical Institute, Katholieke Universiteit Leuven, Celestijnenlaan 200, B-3030 Heverlee, Belgium

⁶ ESTEC Space Science Department, P.O.Box 299, NL-2200 AG Noordwijk, The Netherlands

received May 24 1995, July 15 1995

Abstract. We present a study of low- and high-resolution ultraviolet, high-resolution optical CAT/CES spectra and ultraviolet, optical and infrared photometry of the peculiar supergiant HD 101584. From the photometry we learn that the ultraviolet and optical energy distribution cannot be fitted in a consistent way and we need a model in which the UV and optical energy distribution are formed by different gas. The Geneva photometry is best fitted to a B9II Kurucz model, $T_{eff} = 12000 \pm 1000$ K and $\log g = 3.0 \pm 1.0$, with an extinction of $E(B - V) = 0.49 \pm 0.05$.

The observed spectral features in the spectrum of HD 101584 are classified in eight different categories based on the velocity, shape of profile and the identification. The high-excitation HeI ($\chi = 20.87$ eV), NII ($\chi = 18.40$ eV), CII ($\chi = 14.39$ eV) and NI ($\chi = 10.29$ eV) optical absorption lines are formed in the photosphere of a late B-star (e.g. B8-9I-II). These absorption lines show radial velocity variations which are attributed to binary motion, with the secondary being a white dwarf or a low-mass main sequence object. The low-excitation P-Cygni lines in the optical and UV are formed in the wind. The number density of absorption lines in the UV is so large that the wind spectrum acts as an iron curtain in front of the B-star. The terminal velocity of the wind of $v_\infty = 100 \pm 30$ km s⁻¹ is consistent with the star being a low-mass post-AGB star and the low effective gravity is attributed to the presence of a nearby, unseen, secondary. We estimate a mass-loss

rate of $\dot{M} \approx 10^{-8} M_\odot \text{ yr}^{-1}$. Narrow absorption and emission lines are observed which are formed in a circumsystem disk with a typical radius of $10^2 R_*$.

Key words: line: identification - stars: atmospheres - individual: HD 101584 - mass-loss - peculiar - AGB and Post-AGB

1. Introduction

We have conducted a multiwavelength study of the enigmatic object HD 101584. Classified as a F0Iape (Hofleit *et al.* 1983) it is not a normal F0-type supergiant. The spectrum has many peculiarities, ranging from very narrow optical emission lines of neutral and singly ionized metals (Trams *et al.* 1990), P-Cygni profiles, the HeI 5876 Å absorption line (Morrison and Zimba 1989) to a very large IR excess due to dust (Humphreys and Ney 1974; Parthasarathy and Pottasch 1986; Oudmaier *et al.* 1992). At millimeter wavelengths we find molecular line emission of CO (Trams *et al.* 1990; Loup *et al.* 1990; Van der Veen *et al.* 1993) and OH (Te Lintel Hekkert *et al.* 1992). The very complex structure of the CO emission shows large Doppler velocities of 130 km s⁻¹ with respect to the central velocity of the feature, indicating outflow velocities of more than 100 km s⁻¹. The OH maser line (1667 MHz) emission shows much lower velocities of 30 km s⁻¹ with respect to the same central velocity of 50 ± 2 km s⁻¹.

In the last two decades two models have been developed for HD 101584 and in both models binarity is suggested to explain the observations.

Send offprint requests to: Eric J. Bakker, present address: Astronomy Department, University of Texas, Austin, TX 78712-1083, U.S.A., ebakker@astro.as.utexas.edu

^{*} Based on data collected at the European Southern Observatory (La Silla, Chili), the International Ultraviolet Explorer, IRAS and the Long-Term Photometry of Variables project.

^{**} Table 14 and 15 are also available in electronic form at the CDS via anonymous ftp 130.79.128.5

The first serious model was introduced by Humphreys and Ney (1974). They argue that the infrared radiation is due to the secondary in a binary system. This secondary fills its Roche lobe and material is transferred through the inner Lagrangian point and accreted by the primary. We will show in this paper that this model cannot be supported because we find overwhelming evidence for outflow, rather than for in fall.

A second model was suggested by Parthasarathy and Pottasch (1986) and supported by Trams *et al.* (1991). In this model HD 101584 is in the evolutionary stage of the Post-Asymptotic Giant Branch (post-AGB). During the preceding phase of its evolution on the AGB the star had a strong stellar wind. After the star has left the AGB the expelled material (the AGB remnant) slowly moves away from the star. The dust is in radiative equilibrium with the radiation field of the star, and re-radiates the absorbed energy in the infrared part of the spectrum. The post-AGB nature of HD 101584 is supported by the space velocity of the star derived from the central velocity of the CO and OH millimeter line emission. This velocity of $v_{rad} = 50.3 \pm 2.0 \text{ km s}^{-1}$ does not agree with the galactic rotation curve if the star is at the distance derived by assuming that it is a massive Population I star.

In an attempt to solve the many controversies about this enigmatic star, we have made a multiwavelength study of the ultraviolet, optical and infrared part of the spectrum. Based on these observations we propose a new model for HD 101584.

Sect. 2 gives information about the spectral and photometric data collected and used in this study. In Sect. 3 we look at the total energy distribution and try to fit it with a F0I Kurucz model. In Sect. 4 we distinguish eight different categories of spectral lines and derive for each category a characteristic velocity. In Sect. 5 we converge to consistency between the results of Sect. 3 and Sect. 4 and discuss the nature of HD 101584. Sect. 6 gives the conclusions.

2. The observations

We have collected ultraviolet (IUE), optical (ESO) and infrared (IRAS) spectra completed with optical (Geneva, Strömgen and Johnson) and infrared (near-infrared and IRAS) photometry.

2.1. Ultraviolet spectra

The low-resolution (LORES) ultraviolet spectra of HD 101584 have a wavelength coverage from 1190 Å to 3200 Å with a resolution of $\Delta\lambda = 6.1 \text{ Å}$ for the short-wavelength spectra, and $\Delta\lambda = 9.1 \text{ Å}$ for the long-wavelength spectra. The LORES spectra of HD 101584 were obtained from the IUE archive (SWP31025, LWP10808 and LWP10809 Table 1). A description of the IUE satellite can be found in Boggess *et al.* (1978a and

1978b). The absolute flux calibration of LORES spectra makes it possible to combine it with optical and infrared photometry to make an energy distribution from 1190 Å to 100 μm and to compare the shape of the spectral energy distribution (SED) to Kurucz model atmospheres.

Table 1. Ultraviolet spectra of HD101584

Camera Image No.	Observation Date	Wavelength range [Å]		
Low-resolution IUE spectra				
SWP31025	22 May 1987	1191	-	1950
LWP10808	22 May 1987	1951	-	2551
LWP10809	22 May 1987	2552	-	3199
High-resolution IUE spectra				
LWP17369	15 Febr 1990	2500	-	3000
LWR04822	21 June 1979	2500	-	3000

We used two high-resolution (HIRES) IUE spectra in the long-wavelength range with $\Delta\lambda = 0.3 \text{ Å}$. One HIRES spectrum LWP 17369 was observed by one of us (NRT), whereas the other, LWR04822, was retrieved from the archive at the IUE ground station VILSPA (Spain) (Table 1).

For the identification of the high-resolution UV spectra we made use of a high-resolution spectrum of $\alpha \text{ Lep}$. This F0I type star has the same spectral classification as HD 101584. Comparing the two spectra will enable us to make a quantitative comparison (Sect. 4.4).

2.2. Optical spectra

The optical spectra were obtained with the 1.4 meter Coudé Auxiliary Telescope (CAT) at ESO using the Coudé Echelle Spectrograph (CES) by CW and HvW. Each spectrum has a coverage of about 50 Å with a resolution of $\Delta\lambda = 0.1 \text{ Å}$. These spectra have no absolute flux calibration, so they were normalized to the continuum. Table 2 gives a list of the optical spectra used in this study in order of increasing wavelength.

2.3. Infrared spectra

The low-resolution spectrum (LRS) observed with IRAS was obtained from the archive at Space Research Groningen. The flux scale is absolutely calibrated and the wavelength coverage is from 7 to 24 μm .

2.4. Photometry

From a large set of photometric data available for HD 101584 we have selected the data-points for which the ob-

Table 2. CAT/CES spectra of HD 101584

Date	Observation		δv_{\oplus}^* [km s ⁻¹]	Wavelength range [Å]		Remark
	U.T.	J.D.				
20 Jan. 1990	8h20	7911.847	+19.08	4284	- 4318	
20 Feb. 1989	8h06	7577.838	+15.50	4327	- 4357	H γ
21 Jan. 1990	7h43	7912.822	+19.09	4373	- 4407	
20 Jan. 1990	8h41	7911.861	+19.06	4463	- 4498	MgII
20 Feb. 1989	7h42	7577.821	+15.53	4842	- 4877	H β
19 Feb. 1989	6h28	7576.847	+15.68	5025	- 5064	NII & HeI
13 Feb. 1993	5h55	9031.747	+16.91	5859	- 5911	NaI D & HeI
12 Feb. 1993	6h33	9030.770	+17.02	6537	- 6593	CH & H α
20 Apr. 1992	5h34	8732.732	-01.25	7413	- 7476	NI
13 Feb. 1993	4h12	9031.675	+17.01	8649	- 8721	NI & CaII

* The correction term to convert from observed v_{obs} to heliocentric radial velocity v_{\odot} : $v_{\odot} = v_{obs} + \delta v_{\oplus}$
 To convert to local standard of rest (LSR) velocities $\delta v_{\odot} = 9.22$ km s⁻¹ should be added to v_{\odot}

servation date is closest to the observation date of the LORES UV spectra (Table 3). In this way we minimize the effect of photometric variability of HD 101584 on the composed energy distribution. The UV flux is calculated from the IUE spectra by binning the spectrum in 10 wavelength intervals. The bin with the lowest central wavelength has been rejected as this bin only contains noise. The Geneva photometry is collected by one of us, CW, whereas the Strömgren photometry is taken from the Long Term Photometric of Variables (LTPV) project (Manfroid *et al.* 1991; Sterken *et al.* 1993). The Johnson UVBRI and near-infrared JHKLM photometry are from Trams *et al.* (1991), and the IRAS fluxes from the IRAS point source catalogue (JISWG 1986). The observed magnitudes are converted to a flux scale using the calibration of Rufener and Nicolet (1988) for the Geneva filters, Manfroid *et al.* (1991) for the LTPV Strömgren filters, Landolt-Börnstein (page 73, 1982) for visual Johnson-photometry and Korneef (1983) for near-infrared photometry. The IRAS fluxes are color corrected as described in the IRAS Explanatory Supplement (JISWG 1986).

3. Spectral type from photometry

3.1. The total energy distribution

The energy distribution of HD 101584 is fitted to a Kurucz model atmosphere (Kurucz 1979) with parameters $T_{eff} = 7500$ K and $\log g = 1.0$ which are appropriate for the spectral type of F0I (Hoffleit *et al.* 1983) and the corresponding reddening of $E(B - V) = 0.23$. Fig. 1 shows that we are not able to fit the ultraviolet and optical energy distribution in a consistent way. After normalization at the I-band there is an excess of flux shortward of 1500 Å ($\log \lambda \leq -0.8$ in μm) and an excess at the Balmer jump at 3653 Å ($\log \lambda = -0.4$). The excess shortward of 1500 Å indicates that the star is hotter than F0I.

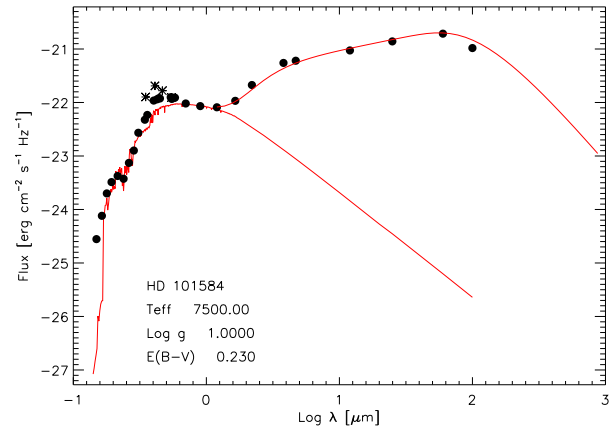


Fig. 1. The complete dereddened energy distribution of HD 101584 with $E(B - V) = 0.230$, ranging from the ultraviolet (1190 Å) to the far-infrared (100 μm). The solid line is a $T_{eff} = 7500$ K, $\log g = 1.0$ Kurucz model. Note the excess of energy at the Balmer jump and at the infrared. The Strömgren photometry is plotted with an asterisk. Their higher flux is due to photometric variability of the star

The huge IR excess indicates the presence of dust. We have tried to fit an optically thin spherically symmetric dust model to the complete energy distribution (Waters *et al.* 1988) (see Fig. 1). From this fit we find that the dust is at a distance between 20 and $10^5 R_*$ with dust temperatures between $T_{dust} = 50$ and 1240 K. If HD 101584 is a $0.54 M_{\odot}$ post-AGB star ($R_* = 38 R_{\odot}$ and $\log L = 3.6$, Boothroyd and Sackmann, 1988) than this yields a total dust mass of $M_{dust} = 2 \times 10^{-2} M_{\odot}$. Taking a gas-to-dust ratio of a hundred gives a total circumstellar mass of $M_{CS} = 2 M_{\odot}$.

Table 3. Observed photometry of HD 101584

Date	λ_c		Magn.	log flux*
Ultraviolet photometry				
22 May 1987	1365 Å			-26.06
JD=6938	1493			-25.28
	1640			-24.84
	1786			-24.42
	1939			-24.25
	2154			-24.25
	2387			-24.17
	2619			-23.75
	2851			-23.45
	3082			-23.09
Geneva photometry				
29 Feb. 1987	3450 Å	<i>U</i>	7.841	-22.78
JD=6865.731	4020	<i>B1</i>	7.322	-22.37
	4250	<i>B</i>	6.421	-22.33
	4480	<i>B2</i>	7.886	-22.29
	5400	<i>V1</i>	7.637	-22.19
	5500	<i>V</i>	6.913	-22.19
	5810	<i>G</i>	8.015	-22.18
LTPV Strömgen photometry				
	3500 Å	<i>u</i>	8.554	-22.34
5 July 1986	4110	<i>v</i>	7.517	-22.09
JD=6617.514	4670	<i>b</i>	7.235	-22.11
	5470	<i>y</i>	6.905	-22.19
Visual Johnson UVBRI band photometry				
30 Jan. 1987	3600 Å	<i>U_j</i>	7.308	-22.67
JD=6836	4400	<i>B_j</i>	7.372	-22.30
	5500	<i>V_j</i>	6.955	-22.22
	7000	<i>R_j</i>	6.689	-22.23
	9000	<i>I_j</i>	6.389	-22.21
Near-infrared photometry				
2 Feb. 1987	1.25 μ m	<i>J</i>	5.975	-22.18
JD=6839	1.65	<i>H</i>	5.152	-22.02
	2.20	<i>K</i>	3.831	-22.71
	3.80	<i>L</i>	1.791	-21.27
	4.70	<i>M</i>	1.112	-21.23
IRAS photometry				
	12 μ m		88.7 Jy	-21.05
	25		133.7	-20.88
	60		177.4	-20.75
	100		98.6	-21.01

* in $\text{erg cm}^{-2} \text{s}^{-1} \text{Hz}^{-1}$

The total amount of observed energy radiated in the infrared of $E = 9.4 \times 10^{-8} \text{ erg cm}^{-2} \text{s}^{-1}$ can be provided by a reddening of $E(B - V) = 0.39 \pm 0.02$ from a spherically symmetric dust shell. This means that the central star has a $(B - V)_o \leq 0.02$ and a spectral type earlier than A0.

We conclude that the optical and UV energy distribution of HD 101584 indicates that the star (or one of the components if it is a binary) is hotter than $T_{\text{eff}} \simeq 7500 \text{ K}$, which is the temperature suggested by its spectral type of F0I. We will show below that the Geneva photometry and

the presence of high-excitation lines in the optical spectrum support this.

3.2. The spectral type from the Geneva photometry

The optical photometry can be used to derive the spectral type of the star. Using the Geneva photometry (Table 3) and the calibration of the Geneva extinction-free parameters X , Y and Z by Cramer and Maeder (1979) we are able to determine the T_{eff} and $\log g$ of the star. The values for HD 101584 are $X = 1.150$, $Y = 0.140$ and $Z = 0.0219$. The value of the Z parameter can be used as a test to determine peculiarities, because the Z parameter is close to zero for normal star while it deviates from zero for peculiar stars e.g. HgMn, Bp and Ap stars. The low value of Z for HD 101584 suggests that the star is not peculiar in the XYZ space. This encourages us to use predicted colors for normal atmospheres to derive the stellar parameters from the Geneva photometry.

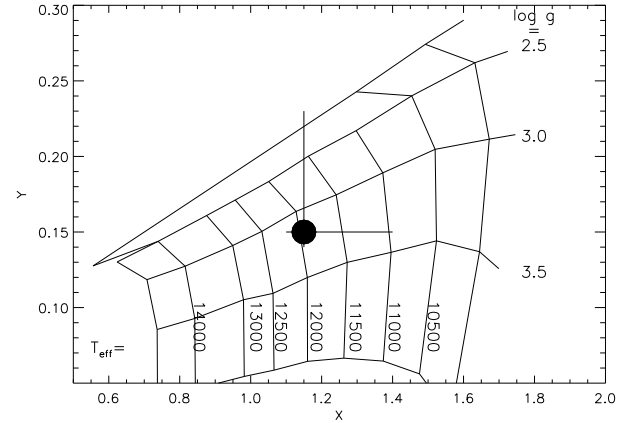


Fig. 2. The Geneva extinction free XY -plane with the position of HD 101584. The grid has been computed with solar metallicity Kurucz models. The best fit is reached for $T_{\text{eff}} = 12000 \pm 1000 \text{ K}$, $\log g = 3.0 \pm 1.0$ and $E(B - V) = 0.49 \pm 0.05$. Note that the error is largest in the direction of lower $\log g$ and lower T_{eff}

We have computed the location of atmospheric models with solar metallicity (Kurucz 1979) in the XY -diagram. (Fig. 2). The location of HD 101584 is closest to the Kurucz model with $T_{\text{eff}} = 12000 \text{ K}$, $\log g = 3.0$ and $E(B - V) = 0.49$.

We will make a rough estimate of the possible error on the derived X and Y of the star caused by the presence of wind lines in the Geneva bands. Only the U and $V1$ band have enough wind lines that the photometry might be effected (the V band is not used for calculating the X , Y and Z parameters). A strong blocking by wind lines would increase the magnitudes of the star compared to

normal stars of the same type. A decrease in flux of 5% in only the U band gives a lower temperature of $T_{eff} = 11500$ K and a surface gravity of $\log g = 2.5$, whereas a decrease in flux of 5% in only the V 1 magnitude yields $T_{eff} = 11000$ K and $\log g \leq 2.0$. A decrease of 5% in both bands gives $T_{eff} = 10000$ K and $\log g \leq 2.0$. This shows that the presence of wind lines in the optical spectrum changes the best fit in the XY -diagram only slightly. We adopt $T_{eff} = 12000 \pm 1000$ K, $\log g = 3.0 \pm 1.0$, and $E(B - V) = 0.49 \pm 0.05$ as the best fit to the Geneva X and Y parameters. This corresponds to a B9II star.

We will show below that this temperature is in good agreement with the spectral type found from photospheric optical absorption lines. The effective gravity which is most affected by blanketing by wind lines is rather uncertain.

4. Line-identification, line profiles and velocities

In this section we will look at the ultraviolet, optical and infrared spectra to learn about different categories of lines which are seen in these spectra. The high-resolution IUE spectrum has been studied by Bakker (1994) and a selected list of line identifications which will be used in this work is given in Table 14 of App. A. We have made a line identification of the optical spectra in selected wavelength regions (Table 2). The identification of the optical spectra as given the Table 15 (App. B) shows absorption lines from high-excitation ($\chi \geq 10.0$ eV), low-excitation ($\chi \leq 10.0$ eV) levels, emission lines from neutral- and singly ionized metals and complex hydrogen line profiles.

The observed spectral features are classified in eight different categories on the basis of the excitation conditions of the atom, shape and velocity of the line profile. To allow comparison between different categories, and observation from different dates, all velocities quoted are heliocentric and to be able to determine velocities relative to the system (star), we have adopted the central velocity of the CO and OH emission, i.e. $+50 \pm 2$ km s $^{-1}$, as the system velocity (see also Sect. 4.8).

We distinguish the following types of spectral lines (Table 4), where we have ordered the categories of lines according to their excitation conditions. Starting with high-excitation lines going down to lower-excitation levels and finishing with molecular lines. In the next section we will argue that this sequence of lines is also a sequence in geometric distance between the line forming region and the central object. Fig. 3 and 4 shows examples of the different categories of lines.

4.1. Type I: Optical pure absorption lines from high-excitation levels

We have detected absorption lines of CII (14.39 eV), HeI (20.87 eV), NII (18.40 eV) and NI (10.29 eV), in the opti-

cal spectrum of HD 101584. This is not consistent with the spectral type of F0Iape as given by Hoffleit *et al.* (1983).

The presence of the CII lines suggests that the optical spectrum (or at least part of it) is produced by a B-type star. For supergiants the CII lines are only formed between types B0.5I and B9I, and reach a maximum strength in B3Ia-type stars (Lennon *et al.* 1992 and 1993). The observed equivalent widths measured for CII(6578) and CII(6583) of 85 and 45 mÅ respectively are of the same order as the equivalent width of a B8.5I and B0.5I star. However as we have also detected NI at the same velocity as HeI and CII we can eliminate the possibility of an early-B type star.

We can obtain additional information by studying the radial velocity of the high-excitation lines. Table 5 gives the observation dates, the average radial velocity on that date and the number of spectral lines (type I) observed on that date. The average radial velocity of all observation dates is 56.9 ± 5.9 km s $^{-1}$. We notice that the difference in velocity between successive observations is much larger than the error ($\approx 7\sigma$) in the individual measurements. As it is unlikely that these high-excitation lines are formed in the stellar wind it is suggestive to attribute the radial velocity variations to the orbital motions of the late-B star around an object whose nature still has to be determined. The amplitude of the radial velocity variations around the system velocity of 50 km s $^{-1}$ is at least 10 km s $^{-1}$. The data for the radial velocity measurements are too scarce to estimate the orbital period.

Table 5. Radial velocities of type I lines

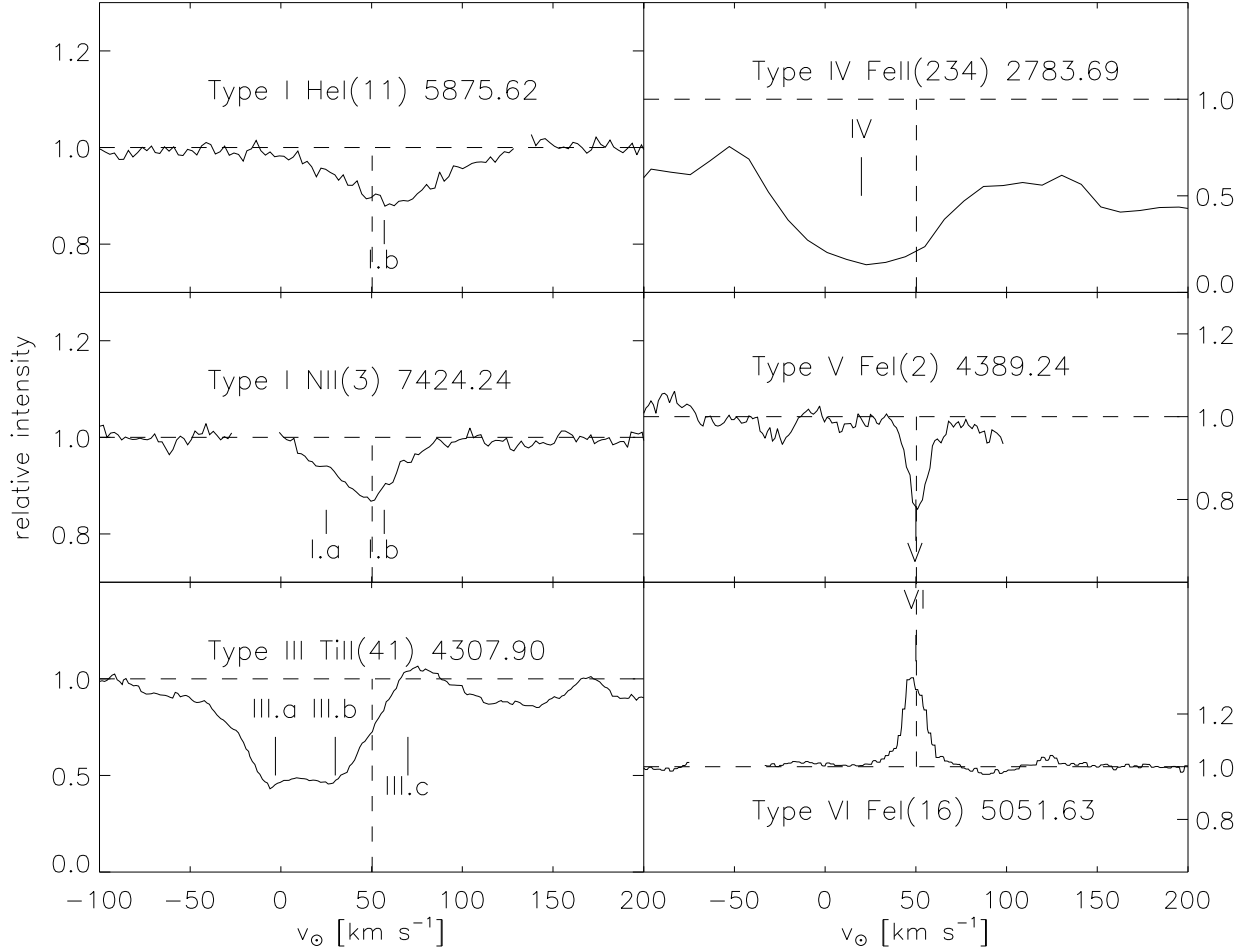
Date	abs. I.a		abs. I.b	
	v_{\odot}	N	v_{\odot}	N
Feb. 1989		00	44.0 ± 2.1	02
Jan. 1990		00		00
Apr. 1992	24.7 ± 1.7	03	54.0 ± 1.7	03
Feb. 1993		00	60.8 ± 0.6	09
Average	24.7 ± 1.7	03	56.9 ± 5.9	14

Of all the high-excitation absorption lines observed only the three NI(mp=3) lines in April 1992 show a second absorption component at 24.7 ± 1.7 km s $^{-1}$ (Table 5). This suggests that the high-excitation absorption lines not only have a variable Doppler velocity, but also a variable line profile.

We conclude that the high-excitation lines in the optical spectrum of HD 101584 are produced in the photosphere of a late-B type star. Its T_{eff} would be between about 10 500 K (B9) and 14 000 K (B5). This is in agreement with the earlier conclusion that the energy distribution indicates $T_{eff} \geq 7500$ K and with the spectral

Table 4. Eight different type of spectral lines are distinguished

Type	Description
I	optical pure absorption lines from high-excitation levels
II	Balmer lines
III	optical P-Cygni lines from low-excitation levels of neutral- and singly ionized metals
IV	ultraviolet absorption lines from low-excitation levels of neutral- and singly ionized metals
V	optical pure absorption lines from low-excitation levels of neutral metals
VI	optical pure emission lines from low-excitation levels of neutral and singly ionized metals
VII	infrared emission feature ($10\ \mu\text{m}$)
VIII	molecular emission lines (CO and OH)

**Fig. 3.** Examples of line types I, III, IV, V and VI

type of B8-9 derived from the Geneva photometry. The star shows radial velocity variations of at least $10\ \text{km s}^{-1}$, which probably indicates the presence of a companion.

4.2. Type II: Hydrogen line profiles and the terminal out-flow velocity

The Balmer lines have a P-Cygni type profile (see Fig. 4 and Fig. 9, 10 and 11) with a strong emission component

($\text{H}\alpha$ and $\text{H}\beta$) and a blue-shifted absorption component (indicated as II.c in Fig. 4). These lines are formed in the stellar wind.

The profile of $\text{H}\alpha$ is complex: a P-Cygni profile superimposed on a very broad emission profile. The emission extends from about -1000 to $+1000\ \text{km s}^{-1}$ (see also Fig. 10 where the width of the $\text{H}\alpha$ emission is of the same order as the total wavelength coverage of the spectrum). It

Table 6. Radial velocities of type II lines

Date		abs. II.a v_{\odot}	abs. II.b v_{\odot}	abs. II.c v_{\odot}	em. II.d v_{\odot}
Feb. 1989	H γ	-58	-10	44	78
	H β	-58	-18	60	82
Jan. 1990					
Apr. 1992					
Feb. 1993	H α		-1	37	83
Average		-58 \pm 2.1	-10 \pm 4.9	47 \pm 4.9	81 \pm 1.5

is most likely due to electron scattering by free electrons in the stellar wind. The absorption wing of H α extends to heliocentric velocity of about -30 km s⁻¹, which corresponds to -80 km s⁻¹ in the frame of the system. The emission component of H β extends to about +180 km s⁻¹, i.e. +130 km s⁻¹ in the frame of the system. This suggests that the P-Cygni profiles are formed in a wind which have a maximum outflow velocity of about 100 \pm 30 km s⁻¹. We will show below that this is similar to the terminal velocity of about 100 km s⁻¹ derived from the P-Cygni profiles of lines from ionized metal in the UV and in the visual, and is similar to the CO outflow velocity.

The profiles of H β and H γ show evidence for two additional absorption components (indicated as II.a and II.b in Fig. 4 and Table 6) at heliocentric velocities of -58 \pm 2 and -10 \pm 5 km s⁻¹, i.e. at -108 and -60 km s⁻¹ in the frame of the system. These components resemble the discrete absorption components that are commonly observed in the profiles of lines formed in stellar winds (Henrichs 1988) and they are interpreted as the result of variable mass loss or density concentrations in the wind.

4.3. Type III: Optical P-Cygni lines from low-excitation levels of neutral and singly ionized metals

In this study we define a line as a P-Cygni type line if the spectral feature shows an absorption (III.b) and an emission (III.c) component with the emission on the long wavelength side of the absorption. The spectrum of HD 101584 shows P-Cygni profiles of lines from low-excitation levels of neutral and singly ionized metals, e.g. FeI, TiI, MnI, NiI and TiII.

Most of the P-Cygni lines show a narrow emission peak (Type VI) superposed on the wider emission of the P-Cygni profile. In some cases it was not possible to distinguish between the pure emission and the emission of the P-Cygni profile. In those cases the two emissions blend together. The weakest P-Cygni type lines clearly show the presence of a second, blue-shifted absorption component (III.a) while for the stronger lines the two absorption components blend together to one broad profile (Fig. 3).

The velocities of the components, derived from multiple Gaussian fits to the profiles, are listed in Table 7. The mean heliocentric velocities of the components III.b and III.c are about +30 and +70 km s⁻¹ respectively. After correction for the system velocity of +50 km s⁻¹, the velocities in the frame of the system are -20 to +20 km s⁻¹. Since the velocities of the emission peak and of the deepest point of the absorption of a P-Cygni profile are not correlated (see e.g. Castor and Lamers 1979) the agreement between these two values can *not* be taken as an indication of the terminal velocity of the wind. The terminal velocity of the wind can be considerably higher than the velocities measured from the peak of the emission and the deepest point of the absorption. The terminal velocity of the wind can be derived from the extent of the blue absorption edge. This is about -50 km s⁻¹ heliocentric velocity, which indicates a terminal velocity of the wind of about 100 km s⁻¹, i.e. about the same as measured from the Balmer profiles.

The profiles show the presence of an extra absorption component at -53 km s⁻¹ in the frame of the system (component III.a in Fig. 3). This component is probably formed in the wind as the P-Cygni profiles of the Balmer lines also showed discrete absorption components.

For those lines of type III that do not show emission, the depth of the III.b absorption component is larger than the depth of the III.a absorption component. However when there is emission in the feature, the III.a component is stronger than the III.b component. This suggests that the emission fills in the III.b component and reverses the ratio of the strength of the two absorption components. In section 4.4 we will see that the UV lines show the same characteristics.

We conclude that the optical lines of neutral and singly ionized metals (type III) show profiles which consist of a P-Cygni profile, formed in a wind with a terminal velocity of about 100 km s⁻¹.

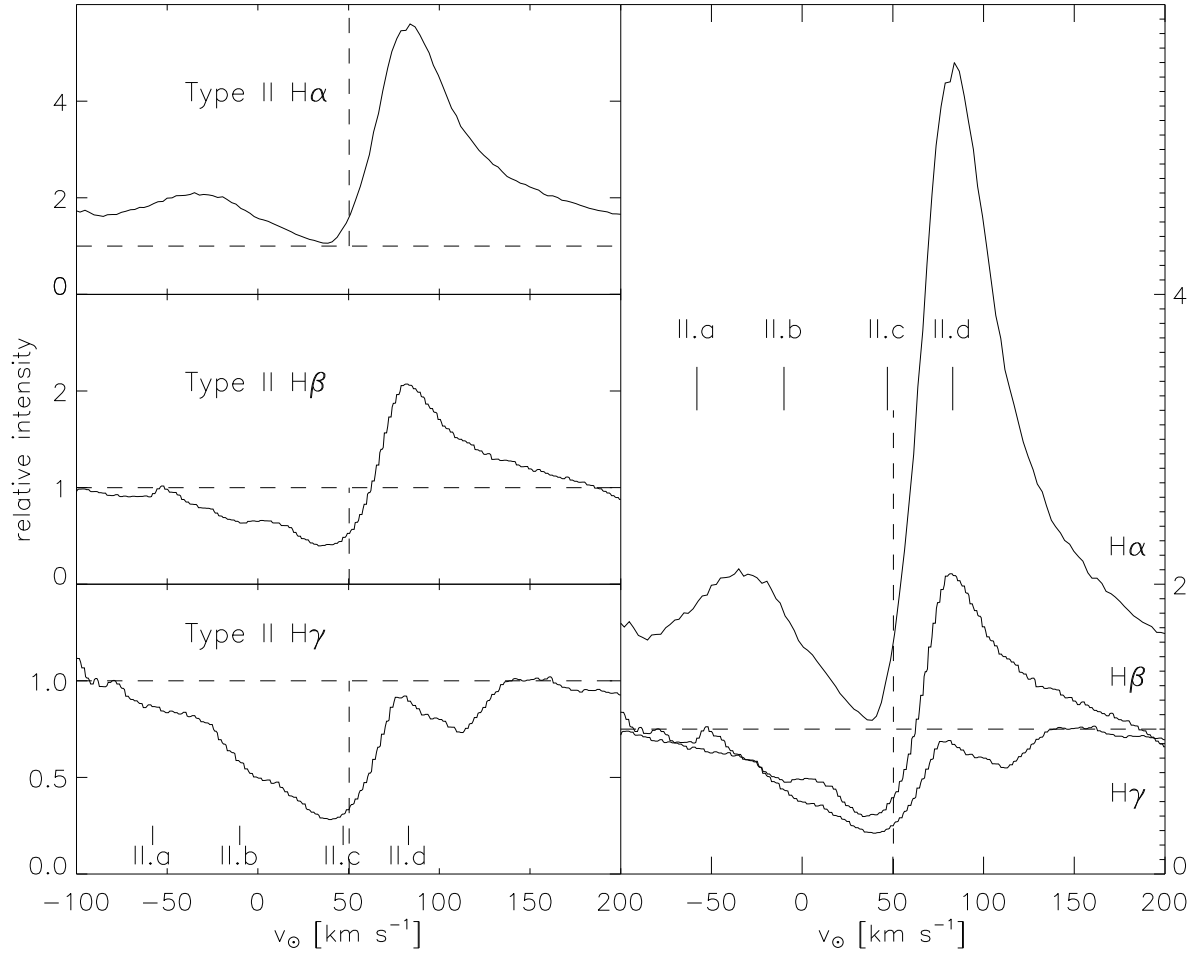


Fig. 4. Hydrogen H α , H β and H γ line profiles. Notice the second absorption component at 0 km s $^{-1}$

Table 7. Radial velocities of type III lines

Date	abs. III.a		abs. III.b		em. III.c	
	v_{\odot}	N	v_{\odot}	N	v_{\odot}	N
Feb. 1989	+0.4 \pm 3.2	09	31.8 \pm 2.4	17	62.3 \pm 4.6	13
Jan. 1990	-4.3 \pm 1.0	27	30.3 \pm 1.1	37	72.9 \pm 4.3	21
Apr 1992		00		00		00
Feb. 1993	-3.5 \pm 1.4	04	24.0 \pm 4.8	05	76.3 \pm 2.3	04
Average	-3.1 \pm 1.8	40	30.2 \pm 2.1	59	69.6 \pm 4.2	38

4.4. Type IV: Ultraviolet absorption lines from low-excitation levels of neutral and singly ionized metals

In an extensive study of the high-resolution IUE spectrum of HD 101584 between 2500 and 3000 Å, 229 absorption features have been identified whereas 41 features remained unidentified (Bakker 1994). The main conclusions are:

(i) the spectrum of HD 101584 has the same absorption features as the FOI star α Lep, but the lines are intrinsically much broader,

(ii) the absorption lines are not symmetric, but have an excess of red absorption (this in contradiction to lines which are formed in a wind which have profiles with additional blue absorption) and

(iii) the spread of 15 km s $^{-1}$ of the Doppler velocities of the cores of the absorption profiles is a factor five larger than measured for the comparison star α Lep (Table 8).

From the list of UV identifications by Bakker (1994) a selection has been made of the FeII lines which are not sig-

Table 8. Radial velocities of type IV lines

Object	Date	v_{\odot}	N
HD 101584	Feb. 1989	17 ± 15	12
HD 101584	Feb. 1990	21 ± 8	19
	Average	20 ± 11	31
α Lep	Dec. 1978	22 ± 3	19

nificantly blended by other lines, and have a secure identification (quality factor $Q = 3$). To prevent the confusion with interstellar absorption lines all lines from the ground level, $\chi = 0.0$ eV, were excluded for this study. The 19 selected FeII line are listed in Table 14.

In this paper we show that the radial velocity of an absorption line of each ion is correlated with the line strength parameter X defined as:

$$\log X = \log gf - 5040 \frac{\chi}{T_{\text{wind}}} \quad (1)$$

This parameter is proportional to the expected column density of the ions (in LTE). Here we will use it as a measure of the optical depth (τ) of a line. From a comparison between the HIRES spectrum of HD 101584 and α Lep no differences in the occurrence of spectral features was found and we adopt the photospheric temperature of a F0Ib star (α Lep) and for the temperature of the expanding photospheric material, $T_{\text{wind}} = 7700$ K.

Fig. 5 shows the correlation between the $\log X$ and the radial velocity for the FeII lines at two different epochs. The mean linear relations between the radial velocity and X are

$$v_{\odot}(\text{FeII}) = -5.48 \times \log X (T_{\text{wind}} = 7700 \text{ K}) + 8.15 \quad (2)$$

on February 15 1990, and

$$v_{\odot}(\text{FeII}) = -12.45 \times \log X (T_{\text{wind}} = 7700 \text{ K}) - 13.47 \quad (3)$$

on June 21 1989.

The radial velocity found for α Lep of 22 ± 3 km s⁻¹ is in agreement with the radial velocity given by Anderson *et al.* (1987) of 24.3 km s⁻¹.

There is clearly a correlation between the $\log X$ and the radial velocity. Other ionization degrees and other species (CrII, MnI etc.) show the same correlation but with slightly different slopes and offsets. We have made the same test on type III lines, i.e. the low-excitation metal lines in the optical, and also found a correlation between $\log X$ and the radial velocity.

We can explain the correlation with a simple model in which the low-excitation UV and optical lines are formed in the wind (Bakker 1993). The stronger the line strength parameter $\log X$ the further out in the wind the line is

formed. The wind accelerates outwards and we expect to see all wind lines to be blue-shifted with respect to the stellar velocity, but the stronger the line, the larger the blue-shift will be.

In this paper we propose a different explanation for the correlation between the line strength and the radial velocity using the results obtained from the optical P-Cygni lines (see Fig. 3 type III), but with the same conclusion that the UV lines are formed in the wind. These optical lines have the same excitation conditions and are from the same species as the UV absorption lines. The optical P-Cygni lines have multiple components. We suggest that the P-Cygni lines in the UV also have multiple components, but that these are not resolved due to a lower resolution of the IUE observations. We only see one broad absorption with the emission component being lost in the continuum. The separation between the two absorption components in the optical lines is 33 km s⁻¹ and the resolution of the IUE spectra is 30 km s⁻¹. So the separation is expected to be barely detectable in the UV lines. A careful examination of the HIRES UV spectra shows that most of the absorption lines indeed show a hint of a second component. This explains the anomalies found in the UV spectrum:

(i) *Large spread in observed radial velocities.* The correlation between $\log X$ and radial velocities introduces a large spread in the average velocity of the UV lines. The average radial velocity of 20 ± 11 km s⁻¹ is in good agreement with the velocity predicted for a blend between III.a and III.b lines.

(ii) *Large equivalent width.* As the absorption lines are the result of two separate absorption components we observe a large equivalent width. Also because of the velocity stratification the absorption is more efficient and optical thickness is reached at a higher column density.

(iii) *Line asymmetry: too much red absorption.* We have seen in the optical spectrum that for the weaker lines the III.b absorption component is stronger than the III.a component. When the emission is important it fills in the III.b component and the III.a component dominates the feature. In fitting a Gaussian to the feature we observe the red component as additional absorption.

From Fig. 5 we learn that the slope and offset of the fit for HD 101584 changes in time (Eq. 2 and 3). This means that the two absorption components move relative to each other or that the emission varies in strength.

The absorption components of the UV P-Cygni profiles extent to a heliocentric velocity of about -50 km s⁻¹ or -100 km s⁻¹ in the velocity frame of the star (Fig. 3). This indicates a terminal velocity of the wind of the star of about 100 km s⁻¹, i.e. the same value as derived from the P-Cygni profiles in the optical.

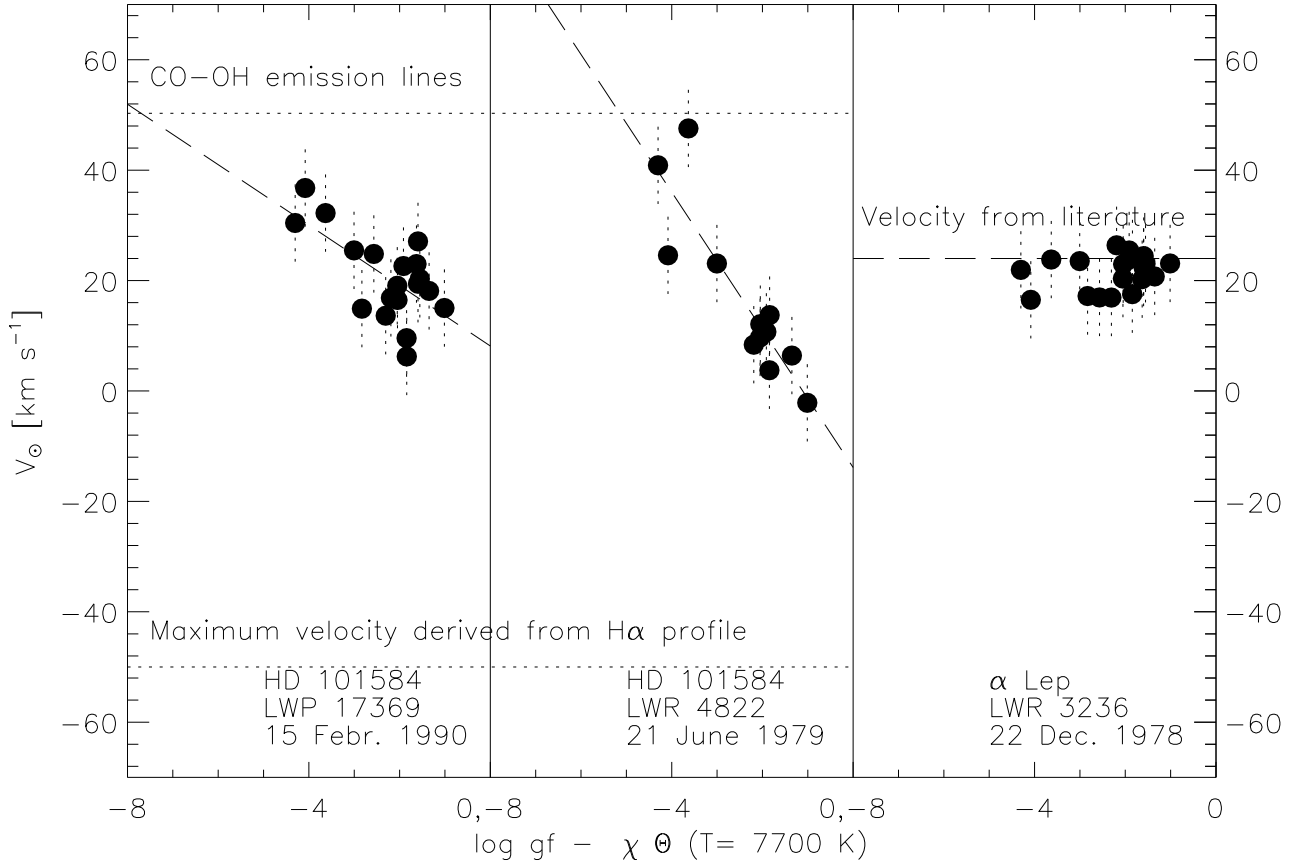


Fig. 5. The correlation between $\log X$ and radial velocity v_{\odot} of UV absorption lines in the spectrum of HD 101584 for two different observation dates. The slope and offset from stellar velocity change in time. The same graph has been made for the reference star α Lep. There is no gradient found in this star

4.5. Type V: Optical pure absorption lines from low-excitation levels of neutral metals

The optical spectra show pure absorption lines from FeI which deviate in shape from all the other absorption features (Fig. 3 type V). The features are much narrower in shape and do not show emission components. The small width of the features and their low-excitation suggest that these lines are formed in a colder region than the other absorption lines.

The radial velocities of these lines are listed in Table 9. The mean radial velocity is $50.4 \pm 1.3 \text{ km s}^{-1}$ (heliocentric) which is exactly equal to the system velocity derived from the CO and OH lines. The radial velocity of the lines does not vary in time. On the basis of their radial velocity, their narrow width and the range of excitation levels ($0.0 \leq \chi \leq 0.22 \text{ eV}$) we argue that these lines are of circumsystem origin and that the gas temperature is lower than the wind and photospheric temperatures, maybe as low as $T_{\text{gas}} \approx 10^3 \text{ K}$.

Table 9. Radial velocities of type V lines

Date	v_{\odot}	N
Feb. 1989	50.5 ± 2.1	02
Jan. 1990	50.3 ± 1.7	03
Apr. 1992		00
Feb. 1993		00
Average	50.4 ± 1.3	05

The only stable geometry which can sustain this material is a (Keplerian) disk with an inclination angle small enough for the line-of-sight to the star to pass through disk material. With a temperature of about $T_{\text{gas}} \approx 10^3 \text{ K}$, the line forming region coincides with the inner region of the dust, i.e. at about $20R_*$ where $T_{\text{dust}} = 1240 \text{ K}$.

The NaI D1 and D2 profiles show a narrow absorption component at a heliocentric velocity of $-32 \pm 2.1 \text{ km s}^{-1}$,

and a velocity in the frame of the system of -82 km s^{-1} . This velocity is rather high for interstellar lines and the same as the edge velocity of the $\text{H}\alpha$ line. Therefore the NaID lines are most likely formed far out in the stellar wind of HD 101584. This implies that we have not detected a single interstellar line in the optical spectrum of HD 101584!

4.6. Type VI: Optical pure emission lines from low-excitation levels of neutral and singly ionized metals

The pure emission lines in the optical spectrum are all from neutral and singly ionized metals like e.g. FeI, TiI, MnI, NiI and TiII, and are hardly resolved in the CAT/CES spectra. (Table 15 shows that the emission lines at 4334 \AA and 7451 \AA have tentatively been identified with LaII and YII respectively. However this identification is uncertain and the lines may be due to unknown metal lines. If this identification is confirmed the presence of these s-elements would pose strict constraints on the evolutionary status of HD 101584).

Table 10. Radial velocities of type VI lines

Date	v_{\odot}	N
Feb. 1989	48.1 ± 0.4	16
Jan. 1990	51.0 ± 3.0	01
Apr. 1992	51.1 ± 0.4	14
Feb. 1993	50.5 ± 0.6	12
Average	49.8 ± 0.6	43

The *FWHM* velocity of the emission lines is 25 km s^{-1} . The average heliocentric velocity of the pure emission lines on the four epochs is $49.8 \pm 0.6 \text{ km s}^{-1}$ (Table 10). Within the error this is equal to the system velocity of $50.3 \pm 2.0 \text{ km s}^{-1}$ derived from the lines of CO and OH. It was already noted by Trams *et al.* (1990) that the radial velocity of the pure emission lines does not vary in time. They argue that these lines are formed either in blobs which were ejected almost perpendicular to the line of sight, or more likely in a distant ring or flattened shell which is tilted towards the observer. We can now exclude the blob interpretation, because we have shown that the same velocity is seen in optical *absorption* lines. We conclude that the narrow optical emission lines are formed in the same circumsystem disk as the optical absorption lines of low-excitation metals. This disk must be seen almost edge-on to account for the low-excitation absorption lines.

The *FWHM* of 25 km s^{-1} of the unresolved emission lines gives a lower limit on the distance between the disk and the star from its Keplerian velocity. If we assume that

the mass of the star or of the binary system is of the order of 1 or $2 M_{\odot}$, we find that the emission lines are formed at a distance of at least 3 AU. Assuming a stellar radius of $R_{*} = 38 R_{\odot}$ for a $0.54 M_{\odot}$ post-AGB stars (Sect. 5) we find that the distance $r_{\text{disk}} \simeq 20 R_{*}$. This distance is the same as the distance found for the inner dust radius derived from the infrared excess (Sect. 3).

4.7. Type VII: Infrared emission feature

The IRAS low-resolution spectrum (LRS, Fig. 6) shows an infrared emission feature. We have fitted this feature with a Gaussian and found a central wavelength of $10.7 \mu\text{m}$. The $10 \mu\text{m}$ feature is attributed to oxygen rich material. This, together with the non-detection of a $11.3 \mu\text{m}$ feature and the detection of OH maser emission indicates that the circumstellar environment is oxygen rich.

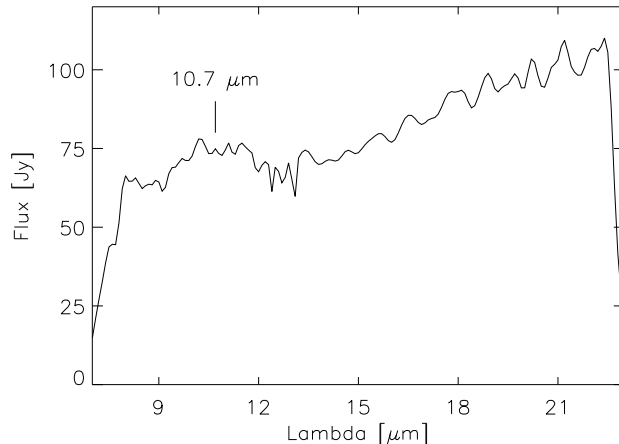


Fig. 6. Low-resolution IRAS spectrum of HD 101584. Notice the detection of a weak $10.7 \mu\text{m}$ infrared feature in emission

4.8. Type VIII: Molecular line emission

HD 101584 shows molecular line emission of $^{12}\text{CO}(J = 1 - 0)$ (2.6 mm) and $^{12}\text{CO}(J = 2 - 1)$ (1.3 mm) (Trams *et al.* 1990; Loup *et al.* 1990), vibrational-rotational bands heads of $^{12}\text{CO}(v'' = 2 - 0)$ ($2.29 \mu\text{m}$), $^{12}\text{CO}(v'' = 3 - 1)$ ($2.32 \mu\text{m}$), $^{12}\text{CO}(v'' = 4 - 2)$ ($2.35 \mu\text{m}$) (Oudmaijer *et al.* 1995) and OH maser emission at 1667 MHz (Te Lintel Hekkert *et al.* 1992). The CO millimeter emission originates from material which is relatively far away from the star ($r \geq 5 \times 10^4 R_{*}$) with temperatures of several tens of K. The OH 1667 MHz main line is formed closer to the star with temperatures on the order of $T_{\text{dust}} \approx 150 - 280 \text{ K}$ (page 247 in Elitzur 1992) at a distance of the order of $r_{\text{OH}} \approx 3 \times 10^3 R_{*}$.

Both CO and OH are integrated over a large volume of emitting material and any asymmetry in the shape or ve-

locity of the emitting volume of material is smeared out in the profile. For this reason we assume that the symmetry axis of the CO and OH line profiles is the radial velocity of the system. Both CO and OH yield the same system velocity with an average value of $50.3 \pm 2.0 \text{ km s}^{-1}$.

CO shows several emission peaks symmetrically around this velocity at a relative velocity to the system of 0, 43 and 130 km s^{-1} . The contribution from the circumsystem disk should be at the system velocity with a width of $\approx 25 \text{ km s}^{-1}$. We identify the central component of the CO emission lines profile as due to the circumsystem disk. The features at 130 km s^{-1} is close to the terminal velocity derived from H α and we identify this component as due to recent mass-loss. The component at 43 km s^{-1} is due to an earlier mass-loss episode of the star (AGB) when the star had a larger radius, a lower escape velocity and thus a lower terminal velocity of the wind.

The CO emission in the near-infrared originates from hot CO gas ($T_{\text{gas}} \approx 2 \times 10^3 \text{ K}$). This temperature is of the same order as the dust temperature in the circumsystem disk which suggests that the near-infrared CO emission originates from the circumsystem disk.

The OH maser 1667 MHz shows a double peaked emission profile with peaks at relative velocity to the system of $\approx 30 \text{ km s}^{-1}$. As this velocity does not corresponds with a CO peak it is unclear where this OH maser originates.

4.9. Summary

The wealth on information on the radial velocities and shapes of spectral lines of HD 101584 gives clues about the nature and geometry of the system. Table 11 gives a summary of the average heliocentric velocities and the velocities in the frame of the system, i.e. relative to the velocity of the CO and OH lines for each category of spectral lines.

5. The nature of HD 101584

In this section we will make a synthesis of the results from the study on the energy distribution and the study on the spectral lines.

5.1. Summary of the observational characteristics

The observations can be summarized as follows and can be visualized with the help of Fig. 8:

1. The CO and OH emission lines show that the system has a heliocentric velocity of $+50 \pm 2 \text{ km s}^{-1}$.

2. The system contains a late type B-star which produces the high-excitation absorption lines in the optical spectrum. The Geneva photometry shows that the star has $T_{\text{eff}} = 12000 \pm 1000 \text{ K}$ and $\log g = 3.0 \pm 1.0$, so it is a late-B star of type about B9. With this gravity the star would be of luminosity class II (see also Fig. 7).

3. This indicates an extinction of $E(B - V) = 0.49 \pm 0.05$.

4. The high-excitation photospheric absorption lines show radial velocity variations with an amplitude of at least 10 km s^{-1} , which suggests that the star has a companion. We will refer to the late-B star as “the primary”. The present data are too scarce to determine a period. However Bakker *et al.* (1995) claim the presence of a 218 day photometric period, and argue that this period is likely present in the Doppler velocities of the high-excitation absorption lines. This strongly support the binary scenario. We did not find any spectroscopic signature of the secondary. This suggests that its visual luminosity would be considerably fainter than that of the primary by at least about a factor 50, which is not exceptional for the companion of a supergiant.

5. The Balmer lines and the low-excitation metal lines in the optical and in the UV show P-Cygni profile. This indicates the presence of a strong stellar wind. This wind is most probably due to the primary because we do not see any spectroscopic evidence for the secondary. The extent of the absorption wings of the P-Cygni profiles of the Balmer lines and the metal lines all indicate a terminal wind velocity, v_{∞} , of about $100 \pm 30 \text{ km s}^{-1}$.

6. The UV spectrum is dominated by the enormous number of metal lines, most of which show P-Cygni profiles. This makes the UV spectrum of HD 101584 to resemble the spectrum of a F-type supergiant although the star has a late-B spectral type (we see an iron curtain in front of the B-star). In fact the UV absorption lines are the same as those observed in the F0Ib supergiant $\alpha \text{ Lep}$, but the lines are stronger in the spectrum of HD 101584 (Bakker 1994). The presence of many P-Cygni profiles and blue-shifted absorption profiles from low-excitation metal lines in the optical spectrum explains the original classification of the star as F0Iape. Fig. 7 displays a 12000 K (B9II) and a 8500 K (A5I) Kurucz model fitted to the dereddened ($E(B - V) = 0.49$) energy distribution of HD 101584. For wavelengths smaller than the Balmer jump the SED resembles a cool A star, while for wavelengths larger than the Balmer jump the SED resembles a hot B star.

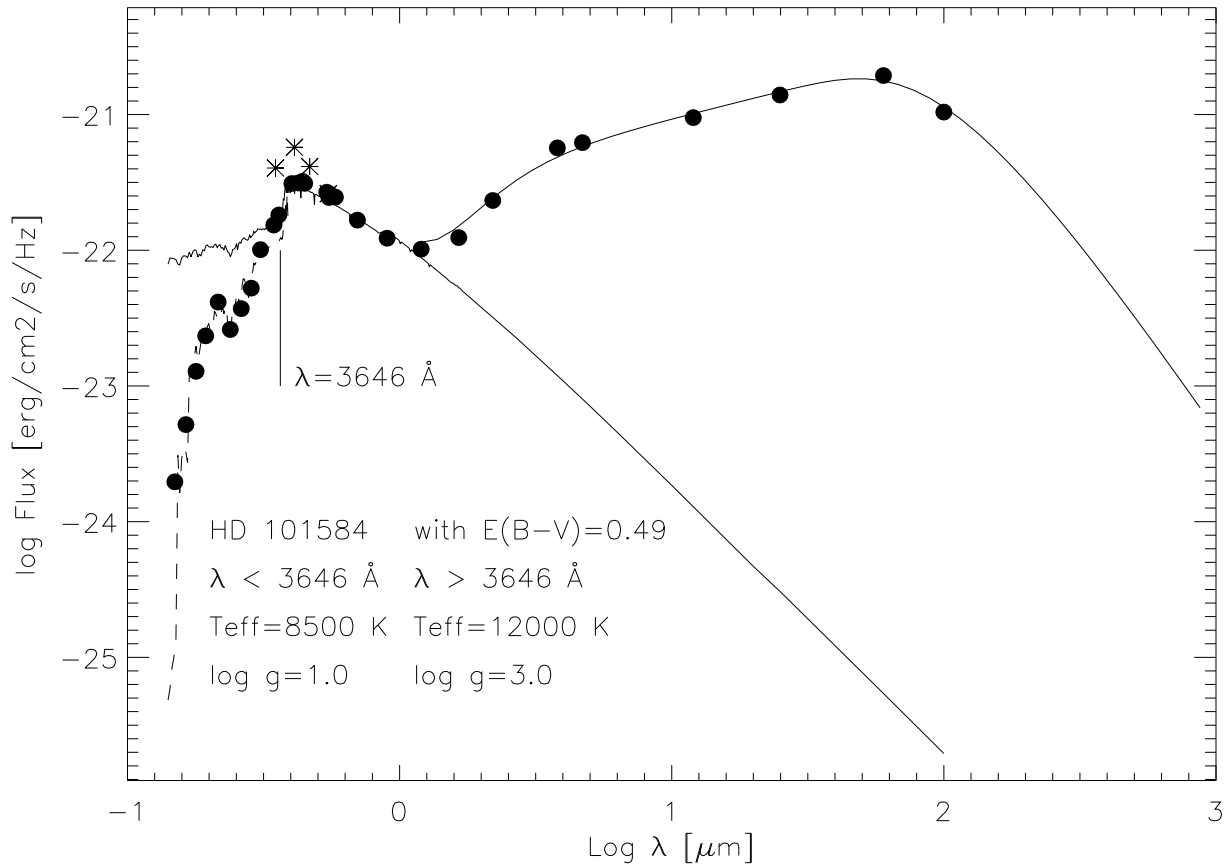
7. The Balmer lines and the wind lines in the optical and in the UV show additional absorption components superimposed on the underlying P-Cygni profiles. These are qualitatively similar to the discrete absorption components observed in the P-Cygni profiles of almost all early type stars. The absorption components in the P-Cygni profiles of HD 101584 are at velocities relative to the star of -20 and -53 km s^{-1} (optical and UV P-Cygni lines) and -108 and -60 km s^{-1} (Balmer lines).

8. The terminal velocity of the wind can be used to derive information about the gravity of the star if we neglect the presence of a companion. The observations of stellar winds of early type stars and the theory of radiation driven winds indicate that v_{∞} is proportional to the photospheric escape velocity, v_{esc} . The ratio $v_{\infty}/v_{\text{esc}}$ is 1.2 ± 0.3 for late-B supergiants (Lamers *et al.* 1995). This implies an escape velocity of $90 \pm 30 \text{ km s}^{-1}$.

Table 11. Heliocentric radial velocities of different categories of spectral lines in the UV and optical spectrum of HD 101584

Category		v_{\odot} [km s ⁻¹]	δv	Remark
I.a	high χ , optical	24.7±1.7	-25±3	abs., only NI(3) at Apr. '92
I.b		56.9±5.9	7±7	abs., B8-9I-II star
II.a	Balmer lines	-58±2	-108±3	abs., shell component
II.b		-10±4.9	-60±5	abs., shell component
II.c		47±4.9	-3±3	abs., wind and photosphere
II.d		81±1.5	+33±3	em., wind in emission
III.a	low χ , optical	-3.1±1.8	-53±3	abs., shell component
III.b		30.2±4.8	-20±5	abs., wind component
III.c		69.6±4.2	20±5	em., wind component
IV	low χ , UV	20±11	-30±11	abs., wind component
V	narrow, low χ , optical	50.4±1.3	0±2	abs., at system velocity
VI	narrow, low χ , optical	49.8±0.6	0±3	em., at system velocity
VII	10 μ m AGB remnant			em., in dusty regions
VIII	CO and OH AGB remnant	50.3±2.0	0±2	em., at system velocity

$\delta v = v_{\odot} - v_{\text{VIII}}$

**Fig. 7.** A B9II (solid line) and a A5I (dashed line, only for $\lambda \leq 3646 \text{ \AA}$) Kurucz models are fitted to the dereddened energy distribution ($E(B-V) = 0.49$) of HD 101584. Due to the many wind lines in the blue and UV part of the spectrum, we observe an iron curtain in front of the B-star and the UV SED mimics an A to F-type star blue-wards of the Balmer jump ($\lambda = 3646 \text{ \AA}$)

9. The optical spectrum shows narrow low-excitation *absorption* lines of neutral Fe at the system velocity. Since these lines are much narrower than the photospheric high-excitation absorption lines and they do not show the radial velocity variations, they must be formed in a circumsystem disk that is in front of the star.

10. The optical spectrum also shows narrow *emission* lines from neutral and singly ionized gas at the system velocity. These lines are formed in the circumsystem gas that also formed the absorptions of the low-excitation FeI lines.

11. The molecular emission of CO in the infrared (vibrational transitions) shows the presence of circumsystem material with a temperature on the order of $T_{\text{gas}} \approx 2 \times 10^3$ K around the system. The emission lines from CO at millimeter wavelengths (rotational transitions) and the OH maser line at 1667 MHz at the system velocity show that the circumsystem gas extends to large distances of about 10^3 to $10^5 R_*$ at temperatures of 10^1 to 10^2 K.

12. The huge infrared excess can be energetically supported by the star if we assume that it has a reddening of $E(B - V) = 0.38 \pm 0.2$ due to a spherically symmetric dust shell. From the IR excess we find that the dust is typically at a distance of 20 to $10^5 R_*$. As the system is seen edge-on the observed reddening will be larger than $E(B - V) = 0.38$. This extinction implies that the star has a spectral type earlier than about A2.

13. The fact that we see the low-excitation FeI lines formed in the circumsystem disk, in *absorption*, means that the line-of-sight to the primary passes through the circumsystem disk. So the disk must be observed almost edge-on. We can then use the width of the circumsystem emission lines of low-excitation metals to estimate the distance from the star. Assuming that the binary system has a total mass of about 1 or 2 M_\odot (see below), the *FWHM* of 25 km s $^{-1}$ of the emission indicates a lower limit on the distance of $20 R_*$. This is of the same order as the dust inner radius.

Fig. 8 shows a simple cartoon of the model of geometry of HD 101584 proposed. This model explains all different categories of spectral lines in a consistent way. We ordered the spectral features in decreasing excitation conditions. This is reflected in the model. The higher the excitation level of the transition, the closer it originates to the central B-star. However this model does not say anything about the evolutionary status (nature) of HD 101584. In the next sections we will use the observations and the model to derive the mass and the nature of HD 101584.

5.2. The mass, luminosity and distance

The stellar wind from HD 101584 has a low terminal velocity of only about 100 ± 30 km s $^{-1}$. This suggests an escape velocity of 90 ± 30 km s $^{-1}$. In Table 12 we give expected parameters for Pop I late-B supergiants and compare these with the data of HD 101584.

The relation between mass and luminosity at $T_{\text{eff}} = 12000$ K was derived from the evolutionary tracks of Schaller *et al.* (1992) under the assumption that the star is moving to the right in the Hertzsprung Russell diagram after it left the main sequence. The radius was derived from L and T_{eff} . The correction factor for the effective gravity due to radiation pressure by electron scattering is $\Gamma = 2.66 \times 10^{-5} L/M$ when L and M are in solar units and hydrogen is supposed to be almost fully ionized in the atmosphere. This is a reasonable approximation for late-B supergiants (Lamers *et al.* 1995).

The escape velocities derived in this way are considerably larger than the observed value of about 90 km s $^{-1}$. This suggests that either the star is even more luminous or that the star is in a later evolutionary phase, and it is evolving to the blue in the HRD after having been a red supergiant.

The distance of the star, derived from L , from the bolometric correction of $BC \simeq -0.70 \pm 0.05$, from $E(B - V) = 0.49 \pm 0.05$ and from $V = 6.95$ is also listed. The distance is between 4 and 11 kpc, which implies a height above the galactic plane between 0.4 and 1.1 kpc.

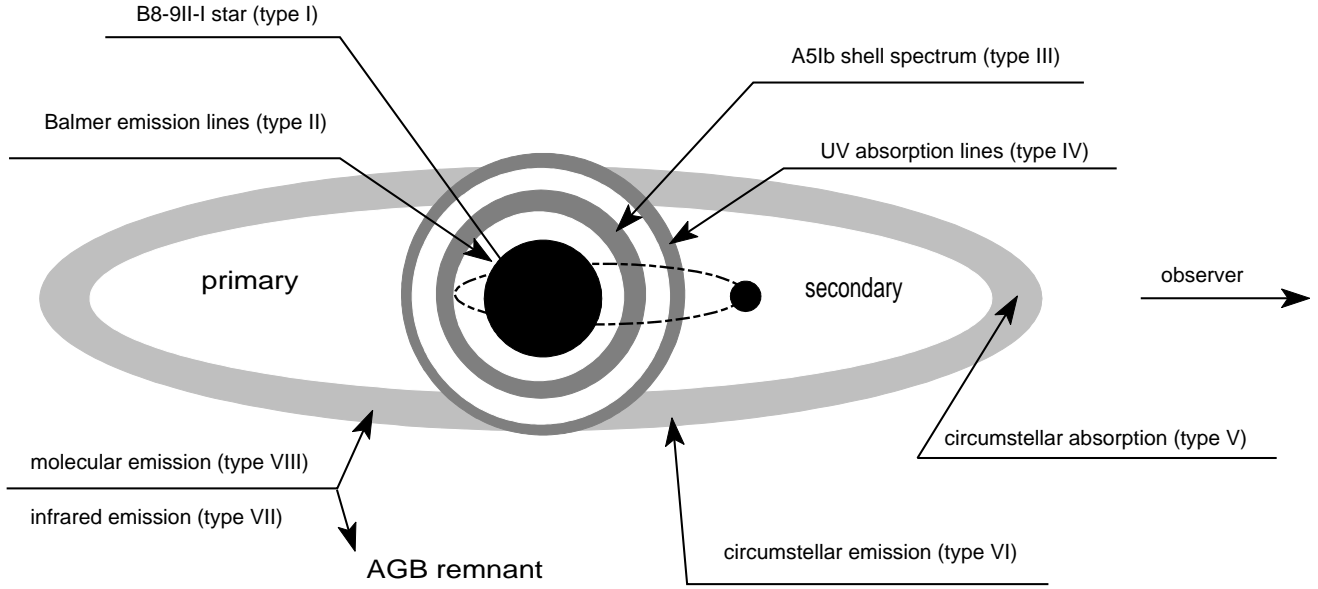
Table 13 gives a similar table in the case that HD 101584 is a post-AGB star. In this case we derive the luminosity from the mass-luminosity relation of Boothroyd and Sackmann (1988). The rest of the data are derived in the same way as for Pop I stars.

Tables 12 and 13 show that an escape velocity of $v_{\text{esc}} = 90 \pm 30$ km s $^{-1}$ is only consistent with Post-AGB stars. The predicted values of v_{esc} of massive stars are about a factor two to three too high. This suggests that HD 101584 is a post-AGB star at a distance between 0.6 and 1.1 kpc. At that distance the star is between 60 and 100 pc above the Galactic plane. The low-mass nature of the progenitor of HD 101584 is in agreement with the galactic latitude and with the high space velocity.

In this discussion we have neglected the role of the companion in the determination of the mass-loss rate and the terminal velocity of the wind. The presence of a circumsystem disk shows that the companion plays or has played a role in the mass-loss history of the star. So the companion may influence the stellar wind, and reduce the effective gravity of the primary and therefore decrease the terminal velocity and increase the mass-loss rate. If this is the case, the low terminal velocity cannot be used as an argument against a massive primary.

5.3. Is HD 101584 a post-AGB binary?

From studies of bright post-AGB stars Waters *et al.* (1993) found that the occurrence of a near-infrared excess is strongly correlated with binarity. The infrared-excess of HD 101584 has a local minimum at $1.25 \mu\text{m}$, which indicates that the circumsystem dust has two components of different temperatures. The total infrared energy distribution can be interpreted as the combination of a near-

**Fig. 8.** A model for HD 101584**Table 12.** Stellar and wind parameters for population I stars

Pop	M_i [M_\odot]	$\log L$ [L_\odot]	M [M_\odot]	R [R_\odot]	Γ	v_{esc} [km s^{-1}]	D [kpc]	v_∞ [km s^{-1}]
I	60	6.00	49.2	230	0.47	210	10.3	227
I	50	5.88	43.3	200	0.40	220	9.0	238
I	40	5.69	36.0	160	0.31	240	7.1	259
I	30	5.47	28.0	130	0.24	250	5.4	270
I	20	5.10	19.0	80	0.15	280	4.1	302

Table 13. Stellar and wind parameters for post-AGB stars

$\log L$ [L_\odot]	M [M_\odot]	R [R_\odot]	Γ	v_{esc} [km s^{-1}]	D [kpc]	v_∞ [km s^{-1}]
4.10	0.70	26	0.43	77	1.1	83
4.00	0.65	23	0.37	83	1.0	90
3.87	0.60	20	0.29	90	0.86	97
3.70	0.55	16	0.22	100	0.71	108
3.52	0.52	13	0.15	114	0.59	123

infrared excess with a dust temperature of $T_{\text{dust}} \approx 1240$ K and a far-infrared excess due to an expanding dust remnant. Dust around a central star of about 12000 K will reach a temperature of 1240 K at an inner dust radius of about $10^2 R_*$.

If HD 101584 is indeed a low-mass post-AGB star it differs from the other post-AGB binaries in that its dust

is O-rich. This can be inferred from the fact that the star shows OH maser lines and the $10 \mu\text{m}$ infrared emission feature. Other post-AGB binaries with a dusty disk, such as HR 4049, HD 213985 and the Red Rectangle (HD 44179), are all surrounded by C-rich dust.

The mass-loss rate of HD 101584 can be estimated by comparing its stellar wind with that of the B8Ia star β Ori

which has a mass-loss rate of $\dot{M} \simeq 10^{-7} M_{\odot} \text{ yr}^{-1}$ and $v_{\infty} \simeq 350 \text{ km s}^{-1}$. The UV spectrum of HD 101584 is similar to that of β Ori, but it shows more blue-shifted UV absorption lines of singly ionized metals (Lamers et al. 1978, Lamers et al. 1995). This means that the column density of the stellar wind of HD 101584 is higher or of the same order of magnitude as that of β Ori. The column density of a stellar wind scales as $N \sim \dot{M} / (v_{\infty} R_*)$, so $\dot{M} \sim N v_{\infty} R_*$. Assuming $R_* = 150 R_{\odot}$ for β Ori and $20 R_{\odot}$ for HD 101584, and $v_{\infty} = 350 \text{ km s}^{-1}$ and 100 km s^{-1} for the two stars respectively we find a rough estimate of \dot{M} (HD 101584) $\geq 4 \times 10^{-9} M_{\odot} \text{ yr}^{-1}$.

The large mass-loss rate of HD 101584, as inferred from the many wind lines, is abnormal for post-AGB stars and suggests a very low effective gravity. This would be consistent with a massive post-AGB star of about $0.7 M_{\odot}$ (see Table 13). However the evolutionary transition time between AGB and Planetary Nebula of a $0.7 M_{\odot}$ post-AGB star is about 10^2 years (Blöcker 1995). This contradicts the fact that the star has not changed its spectral type and visual magnitude in the last 20 years systematically (Humphreys and Ney 1974). Therefore HD 101584 is probably not a massive post-AGB star.

If HD 101584 is a low-mass post-AGB star of $0.5 M_{\odot} \leq M_* \leq 0.6 M_{\odot}$ the higher mass-loss rate and the low effective gravity could be due to the presence of a nearby companion. A decrease of the effective gravity results in an increase of the mass-loss rate and a decrease of the terminal velocity v_{∞} .

We conclude that HD 101584 is probably a post-AGB star (based on its high galactic latitude), of intermediate-mass (based on the fact that it has not shown systematic changes in T_{eff} and M_v) with a nearby companion that affects the stellar wind (based on the high mass-loss rate and low v_{∞}).

6. Conclusions

We have studied the complete energy distribution (1190 Å to 100 μm) and UV, optical and infrared spectra of the enigmatic object HD 101584 and made a consistent model of the geometry of HD 101584 (Fig. 8) and the nature of the observed star. The system contains a cool B-type post-AGB star which probably occurs in a close binary system with a white dwarf or a low-mass main sequence star. The primary suffers from a high mass-loss rate of the order of $\dot{M} \simeq 10^{-8} M_{\odot} \text{ yr}^{-1}$. The very large number of UV metal lines formed in the wind drastically decrease the energy distribution in the UV and hides the B-star behind an iron curtain. The UV spectrum mimics the photospheric spectrum of a F0I star. An upper-limit on the semi-major axis of the system is given by the dust inner radius and is of the order of $10^2 R_*$. The system has a circumsystem disk at a radius of the same order as the dust inner radius. This disk is observed by the detection of narrow emission and absorption lines.

Acknowledgements. The authors would like to thank René Oudmaijer and Lucky Achmad for reading and discussing this paper. The author was supported by grant no. 782-371-040 by ASTRON, which receives funds from the Netherlands Organization for the Advancement of Pure Research (NWO). LBFMW is supported by the Royal Netherlands Academy of Arts and Sciences. This research has made use of the Simbad database, operated at CDS, Strasbourg, France, and the IUE database UNSPL at the University of Utrecht and VILSPA. CAT/CES is operated by ESO. CW thanks the staff of the Geneva Observatory for their kind permission to use the Swiss Telescope at La Silla.

References

- Anderson J., Nordström B., Jensen W.S.: 1987, A&AS 68, 347
- Bakker E.J., 1993: in: "Luminous High-Latitude stars", ASP Conference Series 45, Ed. D.D. Sasselov, page 130-136
- Bakker E.J.: 1994, A&AS 103, 189
- Bakker E.J., Lamers H.J.G.L.M., Waters L.B.F.M., Waelkens C.: 1995, submitted to A&A
- Blöcker T.: 1995, A&A 299, 755
- Boggess A., Carr F.A., Evans D.C. et al. : 1978a, Nature 275, 372
- Boggess A., Bohline R.C., Evans D.C. et al. : 1978b, Nature 275, 377
- Boothroyd A., Sackman J.: 1988, ApJ 328, 641
- Castor J.I., Lamers H.J.G.L.M.: 1979, ApJS 39, 481
- Cramer N., Maeder A.: 1979, A&A 78, 305
- Elitzur M.: 1992, "Astronomical Masers", Astrophysics and space science library, Kluwer Academic Publishers, p. 247
- Henrichs H.: 1988 in: "O stars and Wolf-Rayet stars", NASA SP-497, page 199
- Hoffleit D., Saladyga M., Wlasuk P.: 1983, Supplement to the Bright Star Catalogue, Yale University Observatory, USA
- Humphreys R.M., Ney E.P.: 1974, ApJ 190, 339
- Joint IRAS Science Work Group: 1986, IRAS "catalogues, volume 1-6, Explanatory Supplement and Point Source Catalogue", NASA RP-1190
- Korneef J.: 1983, A&A 128, 84
- Kurucz R.L.: 1979, ApJS 40, 1
- Lamers H.J.G.L.M., Stalio R., Kondo Y.: 1978, ApJ 223, 207
- Lamers H.J.G.L.M., Snow T.P., Lindholm D.M.: 1995, ApJ in press
- Landolt-Börnstein, 1982, "Numerical Data and Functional Relationships in Science and Technology, New Series", Group VI, Vol. 2b., page 73
- Lennon D.J., Dufton P.L., Fitzsimmons A.: 1992, A&AS 94, 569
- Lennon D.J., Dufton P.L., Fitzsimmons A.: 1993, A&AS 97, 559
- Loup C., Forveille T., Nyman L. Å., Omont A.: 1990, A&A 227, L29
- Manfroid J., Sterken C., Bruch A. et al. : 1991, First Catalogue of Stars Measured in the Long-Term Photometry of Variables Project (1982-1986), ESO Scientific Report No. 8, Garching
- Morrison N.D., Zimba J.R.: 1989, BAAS 21, 1022
- Oudmaijer R.D., Van der Veen W.E.C.J., Waters L.B.F.M., Trams N.R., Waelkens C., Engelsman E.: 1992, A&AS 96, 625

- Oudmaijer R.D., Waters L.B.F.M., Van der Veen W.E.C.J., Geballe T.R.: 1995, A&A 299, 690
- Parthasarathy M, Pottasch S.R.: 1986, A&A 154, L16
- Rufener F., Nicolet B.: 1988, A&A 206, 357
- Schaller G., Schaerer D., Meynet G., Maeder A.: 1992, A&AS 96, 269
- Sterken C., Manfroid J., Anton K. *et al.* : 1993, Second Catalogue of Stars Measured in the Long-Term Photometry of Variables Project (1986-1990), ESO Scientific Report No. 12, Garching
- Te Lintel Hekkert P., Chapman J.M., Zijlstra A.A.: 1992, ApJ 390, L23
- Trams N.R., Van der Veen W.E.C.J., Waelkens C., Waters L.B.F.M., Lamers H.J.G.L.M.: 1990, A&A 233, 153
- Trams N.R., Waters L.B.F.M., Lamers H.J.G.L.M., Waelkens C., Geballe T.R., Thé P.S.: 1991, A&AS 87, 361
- Van der Veen W.E.C.J., Trams N.R., Waters L.B.F.M.: 1993, A&A 269, 231
- Waters L.B.F.M., Coté J., Geballe T.R.: 1988, A&A 203, 348
- Waters L.B.F.M., Waelkens C. Trams N.R.: 1993, in: "Mass loss on the AGB and beyond", ed. H.Schwarz, p. 298

A. UV FeII lines

The FeII UV lines used in this paper are from the UV identification table of Bakker (1994). All information about the method used in determining the profile parameters can we found in this article.

B. Complete line identification of the available wavelength intervals from the CAT/CES spectra

This appendix contains the figures of the optical CAT/CES spectra and a complete identification of several of these spectra. The spectra are ordered of increasing wavelength. As not all spectra are from the same date this means that one should be careful in comparing the spectra. From Sect. 4.1 we know that there is some time variability of the observed radial velocities. All radial velocities quoted in this article are corrected to heliocentric velocities.

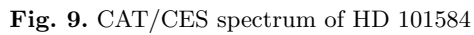
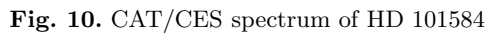


Fig. 9. CAT/CES spectrum of HD 101584



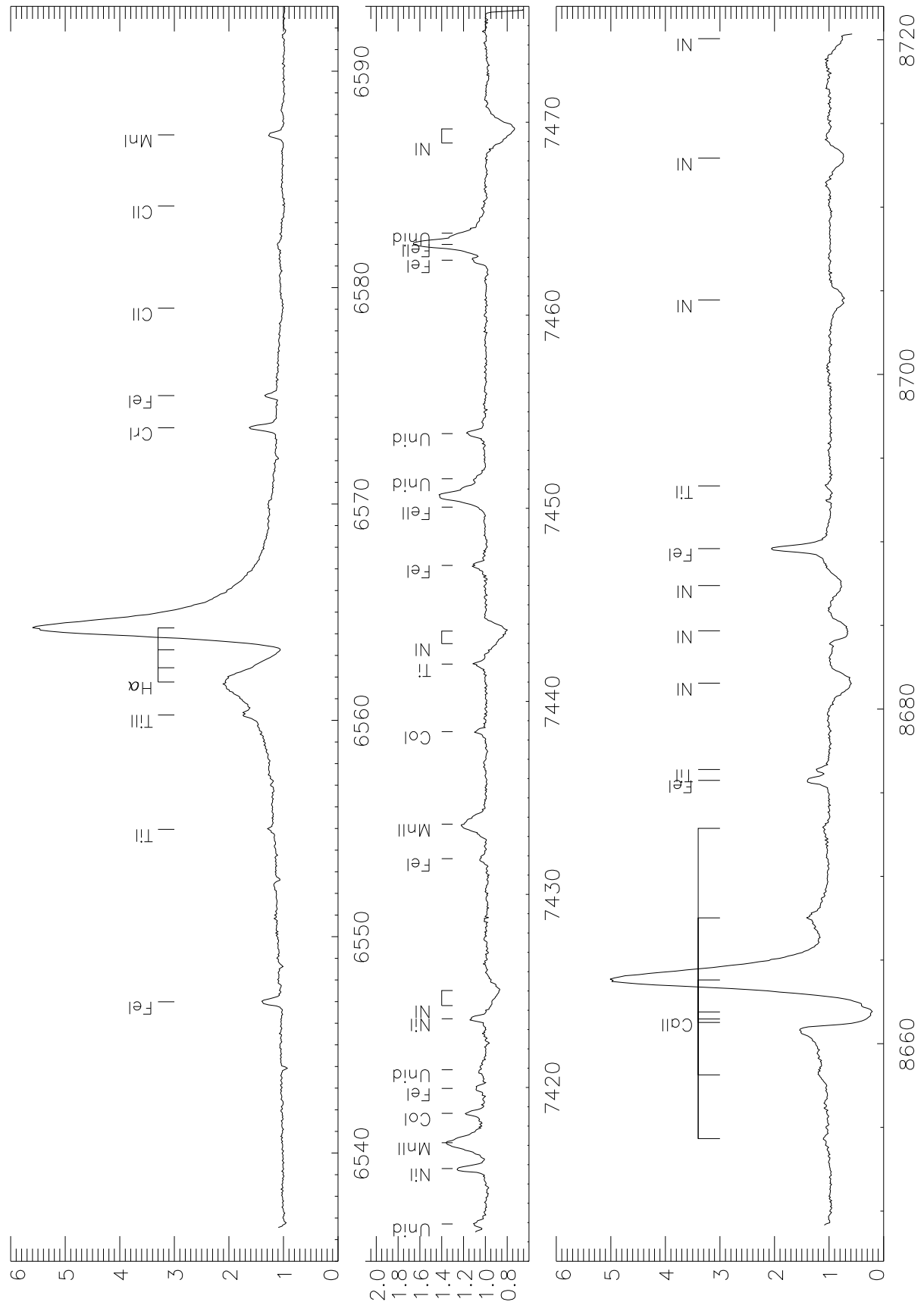


Fig. 11. CAT/CES spectrum of HD 101584

Table 14. 19 selected UV FeII absorption lines of HD 101584 and α Lep

λ_{lab} . [Å]	Multiplet	χ [eV]	$\log gf$	v_{\odot} [km s ⁻¹] *		
				HD 101584		α Lep
				LWP17369	LWR4822	LWR3236
2509.117	242	3.23	-0.89	27	23	24
2513.372	207	3.19	-0.48	26		17
2533.626	159	2.65	+0.14	19		22
2569.775	266	3.41	-1.85	37	25	17
2619.071	171	2.79	-0.48	15		17
2664.665	263	3.37	+0.36	10	4	18
2714.414	063	0.98	-0.37	15	-2	23
2730.735	062	1.07	-0.65	18	6	21
2753.289	235	3.25	+0.50	24		20
2761.813	063	1.09	-0.84	21		23
2767.500	235	3.23	+0.52	28		24
2783.690	234	3.23	+0.20	24	11	25
2880.750	061	0.98	-1.20	7	14	24
2917.465	061	1.04	-2.15	16		17
2926.584	060	0.98	-1.41	19	10	20
2947.658	078	1.66	-0.96	16	12	23
2953.774	060	1.04	-1.51	17	8	26
2986.617	254	3.41	-2.07	30	41	22
2997.298	335	4.48	-0.70	32	48	24

* If the absorption lines is blended or positioned at the end of an echelle no reliable determination of the profile parameters could be made and the item is left blank

Table 15. The optical spectrum of HD 101584

Ident. Ion(mtpl)	λ_{lab} [Å]	χ [eV]	$\log gf$	λ_{obs} [Å]	I		II&III&IV		V abs	VI em	W [mÅ]	Depth [%]	Remark
					abs.	λ_{obs} [km s ⁻¹]	abs.	em					
4284-4318 Å on January 20 1990													
CrII(31)	4284.21	3.84-6.72	-2.25	4284.31			26				200	30	
Unident				4285.13							18	6	
Unident				4285.52							20	6	
VII(23)	4286.13	1.65-4.56	-2.81	4286.22			25				43	15	blended
TiII(20)	4287.893	1.08-3.95	-1.90	4287.54		-6					85	24	
				4288.09			33				224	40	
TiII(41)	4290.222	1.16-4.04	-0.97	4289.93		-1					380	63	
				4290.46			36				251	49	
				4291.16				85			-23	-26	
Unident				4291.91							49	21	
TiII(20)	4294.101	1.08-3.95	-1.05	4293.71		-8					191	43	
				4294.29			32				560	64	
FeII(28)	4296.567	2.69-5.57	-3.36	4296.23		-4						29	
				4296.71			29				346	47	
Unident				4298.15							23	8	noisy
TiII(41)	4300.052	1.18-4.05	-0.47	4299.71		-5					491	77	
				4300.25			32				341	63	
				4300.93				80			-15	-9	
TiII(41)	4301.928	1.16-4.02	-1.28	4301.56		-7					169	37	
				4302.08			30				412	57	
FeII(27)	4303.166	2.69-5.56	-2.53	4303.30			28				557	62	
Unident				4305.69							91	24	broad
TiII(41)	4307.900	1.16-4.02	-1.12	4307.49		-9					234	44	
				4308.02			27				459	58	
				4308.69				74			-34	-6	
Unident				4309.44							134	21	
TiII(41)	4312.861	1.18-4.04	-1.15	4312.51		-5					290	49	
				4313.07			33				375	56	
FeII(32)	4314.289	1.18-4.04	-4.73	4313.77			(-17)					47	blended
				4314.34			23					60	blended
TiII(41)	4314.979	1.16-4.02	-1.18	4314.68		-2						66	blended
				4315.13			30					57	blended
TiII(94)	4316.807	2.04-4.90	-1.70	4316.94			28				210	30	
4327-4357 Å on February 20 1989													
TiII(41)	4330.708	1.18-4.02	-2.08	4330.49			1				82	17	
				4330.94			31				70	20	
Nil(52)	4331.645	1.67-4.52	-1.50	4332.12						48	-43	-14	LaII(24)?
Unident				4334.21							-40	-16	
TiI(20)	4337.916	1.08-3.92	-1.04	4337.81		8					320	53	
				4338.32			44				294	50	
				4338.77				75			-47	-21	
H γ	4340.468	10.15-13.00		4339.41		(-58)					44	10	
				4340.10		-10					44	11	
				4340.88			44				1104	71	
Unident				4341.37				78			-189	-44	
Unident				4342.85							14	4	
Unident				4343.31							47	8	
TiII(20)	4344.291	1.08-3.92	-2.00	4344.22		10					160	18	
				4344.65			40				146	26	
				4345.35				89			-21	-6	
FeI(2)	4347.239	0.00-2.84	-5.69	4347.74					50		42	22	
TiII(94)	4350.834	2.05-4.89	-3.11	4351.01			(28)				26	10	blended
MgI(14)	4351.906	4.33-7.16	-1.72	4351.83		10					417	47	
				4352.27			41				119	19	
				4352.93				86			-154	-15	
FeI(71)	4352.737	2.21-5.05	-1.32	4353.19						47	-37	-15	
4373-4407 Å on January 21 1990													
FeI(648)	4374.495	3.29-6.11	-2.54	4374.08		-9					50	17	
				4374.65			30				413	52	
Unident				4375.64				98			-40	-22	
				4379.47							18	7	NeII(56)?
				4379.90							134	33	
FeI(41)	4383.547	1.48-4.29	-0.09	4379.88		-6					-157	-28	
				4383.18			27				76	22	
Unident				4383.67							255	38	
FeII(27)	4385.381	2.77-5.58	-2.63	4384.54							71	18	
				4384.95		-10					88	29	
				4385.50			27				275	50	
TiII(104)	4386.858	2.59-5.40	-0.79	4386.18		1					-31	-11	
				4386.60			26				14	5	
				4386.96							114	24	
				4387.68				75			-21	-7	
FeI(2)	4389.244	0.05-2.86	-4.57	4389.71					51		45	22	narrow
TiII(61)	4390.977	1.23-4.04	-1.23	4390.66		-3					56	10	
				4391.13			30				136	23	
				4391.72							-181	-25	
Unident				4393.85							135	24	
TiII(19)	4395.031	1.06-3.89	-0.55	4394.65		-7					476	71	
				4395.30			37				449	62	
				4396.30				106			-82	-19	
TiII(51)	4399.767	1.23-4.04	-1.32	4399.43		-4					146	33	
				4399.99			34				420	58	
				4400.60			(76)				99	25	
				4401.16				114			-52	-12	
FeI(41)	4404.752	1.55-4.35	-0.57	4404.44		-2					41	13	
				4404.86			26				119	26	
				4405.68				82			-73	-13	
4463-4498 Å on January 20 1990													
TiII(40)	4464.458	1.16-3.92	-1.62	4464.10		-5					40	14	
				4464.63			30				263	36	
				4465.17				67			-118	-20	
Nil(168)	4466.394	3.69-6.45	+0.02	4466.25		9					20	6	
				4466.83			48				59	13	
TiII(31)	4468.493	1.13-3.89	-0.63	4466.93				55			-46	-17	
				4468.07		-9					221	53	
				4468.75			36				656	74	
TiII(40)	4470.864	1.16-3.95	-2.05	4469.38				79			-425	-48	
				4470.51		-5					21	9	
				4470.98			27				138	27	
FeI(2)	4471.68	0.11-2.87	-6.20	4471.61				69			-4	-2	narrow
				4472.13					49		69	26	

Table 15. continued

Ident. Ion(mtpl)	λ_{lab} [Å]	χ [eV]	$\log gf$	λ_{obs} [Å]	I abs.	II&III&IV			V abs.	VI em	W [mÅ]	Depth [%]	Remark
						abs.	abs [km s ⁻¹]	em					
FeII(37)	4472.921	2.83-5.59	-4.31	4473.04			27				148	25	
				4473.45				55			-115	-13	
FeI(350)	4476.021	2.83-5.59	-0.67	4476.07			22				18	4	
				4476.32			39				46	18	
				4476.42				46			-91	-28	
Unident				4478.87							25	6	
				4479.42							7	2	
MgII(4)	4481.129	8.83-11.58	+0.74	4481.37			35				614	59	
MgII(4)	4481.327	8.83-11.58	+0.59	4481.84			53				34	19	
FeI(68)	4482.257	2.21-4.97	-1.45	4482.73					51		-45	-21	
TiII(115)	4488.319	3.11-5.86	-0.62	4487.92		-8					62	11	blended
				4488.53			33				241	36	blended
FeII(37)	4489.185	2.82-5.57	-3.50	4488.97		5					44	13	blended
				4489.32			28				166	35	blended
				4490.20				87			-118	-29	
FeI(2)	4489.741	0.12-2.86	-3.98	4490.22					51		108	38	narrow
FeII(37)	4491.401	2.84-5.59	-2.89	4490.99		-8					45	13	
				4491.50			26				341	43	
				4492.16				70			-53	-12	
TiII(18)	4493.53	1.08-3.82	-3.62	4493.05		-13					38	8	
				4493.57			22				55	12	
				4494.00				50			-29	-18	
FeI(68)	4494.568	2.19-4.93	-1.07	4494.31		2					10	5	
				4494.64			24				30	10	
				4495.00				48			-45	-23	
MnII(17)	4496.989	10.60-13.35	-0.92	4496.73		2					23	10	
				4497.02			21				72	13	
				4497.42				48			-23	-8	
4842-4877 Å on February 20 1989													
Unident				4843.69							-7	-5	
CrII(30)	4848.24	3.85-6.39	-1.40	4848.55			35				222	30	
TiII(29)	4849.18	1.13-3.67	-2.98	4849.71					48		-93	-30	YII(22)?
Unident				4855.36							-26	-13	
Unident				4856.00							-24	-10	
H β	4861.332	10.15-12.69		4860.13		(-58)					80	11	weak
				4860.79		-18					181	27	
				4862.04			(60)				1163	88	
				4862.40				82			-1266	-175	
CrII(30)	4864.32	3.84-6.39	-1.66	4864.57			31				130	27	
				4865.00			(58)				45	12	
TiII(29)	4865.620	1.11-3.65	-2.72	4866.16					49		-124	-49	
Unident				4866.77							-22	-6	
CoI(158)	4867.870	3.10-5.65	0.27	4868.38					47		-12	-6	
FeI(318)	4871.323	2.85-5.39	-0.54	4871.83					47		-48	-20	
FeI(318)	4872.144	2.87-5.40	-0.28	4872.65					46		-32	-12	
TiII(114)	4874.025	3.08-5.88	-0.99	4874.25			30				48	14	
				4874.63			(53)				26	8	
CrII(30)	4876.41	3.84-6.37	-1.70	4876.72			34				178	26	
5025-5064 Å on February 19 1989													
TiI(38)	5024.842	0.81-3.29	-0.52	5025.39					48		-7	-4	
FeI(1065)	5027.136	4.14-6.59	-0.91	5026.96		5					8	2	
				5027.39			31				1	3	
				5027.71				50			-8	-3	
FeI(791)	5028.129	3.56-6.01	-1.34	5028.70					50		-23	-8	
FeI(718)	5029.623	3.40-5.85	-1.90	5030.22					51		-15	-5	
Unident				5030.81							34	8	
				5031.21							118	22	
				5032.02							-67	-1	
Unident				5033.18							35	6	CII(17)?
Unident				5034.43							24	3	hot star
NII(143)	5035.374	3.62-6.07	+0.38	5035.73			37				15	4	
				5035.92				48			-12	-5	
TiI(110)	5036.468	1.44-3.89	+0.32	5036.22		1					42	1	
				5036.56			21				11	3	
FeI(465)	5036.931	3.00-5.45	-3.30	5037.11			26				4	2	
				5037.50				50			-36	-13	
TiII(71)	5037.81	1.57-4.02	-3.56	5038.36					48		-17	-6	
TiI(110)	5038.400	1.42-3.87	+0.21	5038.97					50		-11	-5	
Unident				5039.77							29	5	hot star
SiII(5)	5041.063	10.02-12.47	+0.28	5041.57			46				251	20	
				5041.65				51			-62	-30	
FeI(36)	5041.759	1.48-3.93	-2.78	5042.30					48		-81	-33	
Unident				5043.94							17	2	hot star
TiI(38)	5043.578	0.83-3.28	-1.65	5044.14					49		-13	-5	
NII(4)	5045.098	18.40-20.85	-0.39	5045.59	45						44	5	
HeI(47)	5047.736	21.13-23.57	-1.60	5048.20	43						59	6	
FeI(114)	5049.825	2.27-4.71	-1.32	5049.74			11				11	2	
				5050.38				49			-68	-23	
FeI(16)	5051.636	0.91-3.35	-2.45	5052.20					49		-85	-33	
TiI(199)	5052.879	2.17-4.61	-0.31	5052.89			16				11	3	
				5053.45				50			-11	-4	
SiII(5)	5056.020	10.03-12.47	+0.54	5056.58				49			332	32	broad
SiII(5)	5056.353	10.03-12.47	-0.42	5056.58									
FeI(1)	5060.079	0.00-2.44	-6.16	5060.68					51		49	21	narrow
TiI(199)	5062.112	2.15-4.59	-0.47	5061.80		-3					3	1	
				5062.24			23				34	5	
				5062.75				53			-8	-3	
5859-5911 Å on February 13 1993													
Unident				5863.16							-40	-5	broad
Unident				5864.40							-12	-3	
TiI(72)	5866.453	10.6-3.17	-0.80	5867.11					51		-19	-8	
HeI(11)	5875.618	20.87-22.97	+0.74	5876.48	61						135	12	
NaI(1)D2	5889.953	0.00-2.10	+0.11	5888.98					(-33)		152	83	CS
				5889.51		-6					405	75	
				5890.05			22				583	57	
				5891.10				75			-271	-33	
NiI(68)	5892.878	1.98-4.07	-1.36	5893.57					52		-39	-14	
NaI(1)D1	5895.923	0.00-2.09	-0.19	5895.01					(-30)		160	88	CS
				5895.58		-1					409	80	
				5896.20			31				512	46	
				5897.00				72			-277	-27	
TiI(71)	5903.317	1.06-3.15	-1.90	5903.85					(44)		41	5	wrong?

Table 15. continued

Ident. Ion(mtpl)	λ_{lab} [Å]	χ [eV]	$\log gf$	λ_{obs} [Å]	I abs.	II&III&IV			V abs.	VI em	W [mÅ]	Depth [%]	Remark
						abs.	abs.	em [km s ⁻¹]					
6537-6593 Å February 12 1993													
FeI(268)	6546.245	2.75-4.63	-1.72	6546.99						52	-21	-4	
TiI(102)	6554.226	1.44-3.32	-1.28	6554.96						51	-22	-11	
TiII(91)	6559.580	2.04-3.92	-2.14	6560.25						48	-54	-20	
H α	6562.817	10.15-12.04		6561.77		-31							edge
				6562.43		-1							
				6563.26			37						abs. min.
				6564.27				83					abs. max.
CrI(16)	6572.900	1.00-2.88	-4.01	6573.52						45	-165	-39	
FeI(13)	6574.238	0.99-2.85	-5.02	6575.01						52	-54	-20	
CII(2)	6578.03	14.39-16.26		6579.05	64						85	5	
CII(2)	6582.85	14.39-16.26		6583.77	59						45	2	
MnI(51)	6586.343	4.41-6.28	-2.01	6587.06						50	-91	-29	
7413-7476 Å on April 20 1992													
Unident				7412.93							-41	-11	
NI(62)	7414.51	1.98-3.64	-2.77	7415.80						51	-95	-28	
MnII(4)	7415.78	3.69-5.35	-2.46	7417.14						54	-306	-36	broad
CoI(89)	7417.38	2.03-3.70	-2.42	7418.66						51	-69	-19	
FeI(1001)	7418.674	4.12-5.79	-1.17	7419.95						50	-38	-10	
Unident				7420.92							-44	-6	
NI(139)	7422.30	3.62-5.28	+0.06	7423.56						50	-46	-15	
NI(3)	7424.24	10.28-11.94	-0.61	7424.24	(23)						13	4	
				7425.02	55						123	12	
FeI(204)	7430.58	2.58-4.24	-3.81	7431.85						50	-21	-6	
MnII(4)	7432.27	3.69-5.35	-2.79	7433.64						54	-199	-23	broad
CoI(53)	7437.16	1.95-3.61	-3.64	7438.43						50	-34	-10	
Ti(225)	7440.600	2.25-3.90	-1.19	7441.93						52	-34	-10	
NI(3)	7442.28	10.29-11.94	-0.31	7442.99	(27)						58	8	
				7443.64	54						142	19	
FeI(1077)	7445.776	4.24-5.90	-0.13	7447.04						50	-52	-13	
FeII(73)	7449.34	3.87-5.53	-3.60	7450.06						51	-332	-42	broad
Unident				7451.53							-50	-10	YII(25)?
Unident				7453.87							-70	-18	
FeI(204)	7461.534	2.55-4.20	-3.48	7462.85						52	-44	-13	
FeII(73)	7462.38	3.87-5.53	-2.98	7463.67						51	-377	-63	broad
Unident				7464.25							-159	-20	
NI(3)	7468.29	10.28-11.94	-0.13	7468.92	(24)						63	8	
				7469.65	53						251	25	
8649-8721 Å on February 13 1993													
CaII(2)	8662.140	1.69-3.11	-0.73	8661.48		-6						71	rel. min.
				8661.90			9					77	abs. min.
				8661.27			21					65	rel. min.
				8663.81				75				-400	abs. max.
				8658.14						(-122)		-18	-172 km/s
				8667.52						(203)		-37	153 km/s
				8654.33						(-253)		-1	-303 km/s
				8672.87						(339)		-6	289 km/s
FeI(339)	8674.751	2.82-2.42	-1.89	8675.74						51	-183	-41	
TiI(68)	8675.38	1.06-2.48	-1.30	8676.39						52	-87	-24	
NI(1)	8680.24	10.29-11.71	+0.42	8681.55	62						525	40	
NI(1)	8683.38	10.29-11.71	+0.14	8684.68	62						435	35	
NI(1)	8686.13	10.29-11.70	-0.27	8687.38	60						299	22	
FeI(60)	8688.633	2.17-3.59	-1.41	8689.59						50	-550	-107	
TiI(68)	8692.34	1.04-2.46	-1.92	8693.34						52	-15	-6	
NI(1)	8703.24	10.29-11.70	-0.27	8704.45	59						365	27	
NI(1)	8711.69	10.29-11.70	-0.16	8712.93	60						329	28	em. on wings
NI(1)	8718.82	10.29-11.71	-0.23	8720.07	60						280	23	